Biochimica et Biophysica Acta 1860 (2016) 795–801

Contents lists available at ScienceDirect

Biochimica et Biophysica Acta

journal homepage: www.elsevier.com/locate/bbagen

Insights into the interaction of the N-terminal amyloidogenic polypeptide of ApoA-I with model cellular membranes

Giulia Rusciano [a,*], Giuseppe Pesce [a], Gianluigi Zito [a], Antonio Sasso [a], Rosa Gaglione [b], Rita Del Giudice [b], Renata Piccoli [b,c], Daria Maria Monti [b,c], Angela Arciello [b,c]

[a] Department of Physics E. Pancini, University of Naples Federico II, via Cintia, 80126-I, Naples, Italy
[b] Department of Chemical Sciences, University of Naples Federico II, via Cintia, 80126-I, Naples, Italy
[c] INBB, Istituto Nazionale di Biostrutture e Biosistemi, Italy

ARTICLE INFO

Article history:
Received 4 September 2015
Received in revised form 27 December 2015
Accepted 6 January 2016
Available online 25 January 2016

Keywords:
Amyloidosis
Raman tweezers
ApoA-I
Model membranes
Lipid phases

ABSTRACT

Background: About twenty variants of apolipoprotein A-I (ApoA-I) are associated to hereditary systemic amyloidoses. Although the molecular bases of this disease are still largely unknown, it has been hypothesized that ApoA-I proteolysis is a key event in pathogenesis, since it triggers the release of an N-terminal fragment (80–100 residue long) that misfolds to form amyloid deposits in peripheral organs and tissues. It is also known that cell membrane lipids play a key role in the fibrillogenic pathway. In the case of ApoA-I related amyloidosis caused by L174S mutation, the 93-residue N-terminal fragment of ApoA-I ([1-93]ApoA-I) was found to be the major constituent of *ex vivo* fibrils.
Methods: With the main goal to investigate the interaction of either [1-93]ApoA-I and ApoA-I with biomimetic membranes, we set-up an experimental system based on the Raman Tweezers methodology. We tested GUVs composed by two types of zwitterionic lipids with a different fluidity degree, *i.e.* dioleoylphosphatidylcholine (DOPC) and dipalmitoylphosphatidylcholine (DPPC).
Results: We found that [1-93]ApoA-I induces conformational disorder in an ordered lipid bilayer. When interacting with fluid phases, instead, the fragment was found to be able to penetrate the membrane bilayer inducing an alignment of lipid chains.
Conclusions: The interaction features of [1-93]ApoA-I with biomimetic membranes strongly depend on the lipid phase. Full-length ApoA-I was found to have similar effects, even if significantly less pronounced.
General significance: Our observations shed light on still largely unknown molecular bases of ApoA-I fibrillogenic domain interaction with membranes.

1. Introduction

It is known that the interaction of proteins with chemical groups exposed on a membrane surface is able to modify their conformational states [1–3]. On the other hand, it has also been reported that proteins can alter membrane fluidity, and/or permeate the membrane bilayer, eventually extracting membrane lipids [4]. In the case of natively unfolded polypeptides, it has been demonstrated that, upon interaction with surfaces, they readily adopt helical structures that represent key intermediates in the amyloid formation process [5]. In particular, anionic surfaces and anionic phospholipid-rich membranes can play key roles either in triggering protein–protein aggregation (fibrillogenesis) by acting as conformational catalysts for amyloid fibril deposition [1], or as inhibitors of fibrillogenesis [6].

Membranes also play a key role in amyloidoses associated with specific variants of apolipoprotein A-I (ApoA-I), the major structural component of high density lipoproteins (HDL). Specific ApoA-I mutations are responsible for well-known familial systemic amyloidosis [7], characterized by amyloid deposition in peripheral organs, such as heart, liver or kidneys. In rarer cases, amyloid is also found in the testes and adrenal glands [7–9]. Notably, the molecular bases of the onset and development of this pathology are still largely unknown.

The prevailing concept in this field is that ApoA-I proteolysis is a key event in the development of the disease, since it triggers the release of the N-terminal fragment (80–100 residue long) that misfolds to form amyloid deposits [10]. In both lipid-bound and lipid-free ApoA-I, this region 80–100 forms well-ordered helical structures [11–13] and is expected to be protected from proteolysis. Nevertheless, it is emerging that a single point amyloidogenic mutation is able to profoundly alter the protein 3D structure, thus presumably exposing protein regions to proteolytic attack. In ApoA-I amyloidosis caused by the presence of L174S mutation, the 93-residue N-terminal polypeptide of ApoA-I (henceforth denoted as [1-93]ApoA-I) was found to be the major constituent of *ex vivo* fibrils [14]. Recently, we produced a recombinant

* Corresponding author.
E-mail address: giulia.rusciano@unina.it (G. Rusciano).

http://dx.doi.org/10.1016/j.bbagen.2016.01.010
0304-4165/

version of this polypeptide, which was found to be natively unfolded in aqueous solutions at pH 7.0 [15]. Upon acidification to pH 4.0, we observed a conformational transition towards a helical state, which we have proposed to be a key intermediate in the fibrillogenic pathway, leading to the formation of a β-sheet-based polymeric structure that evolves into typical amyloid fibrils [15]. Moreover, we also demonstrated that a lipid environment induces and stabilizes helical intermediates of [1-93]ApoA-I, thus affecting its aggregation pathway [16]. This is noteworthy considering that ApoA-I functional role is strictly related to its interactions with lipids and that the N-terminal region of ApoA-I contributes to the binding of the native protein to lipids [17–18]. In particular, cholesterol, a natural ApoA-I ligand, is able to induce a transition towards a helical conformation and to inhibit protein aggregation in a concentration- and time-dependent manner [16]. Similar to cholesterol, zwitterionic, negatively and positively charged liposomes were found to be able to increase the helical content, with negatively charged liposomes showing the greatest effect in inducing helical species [16].

The work presented herein is committed to shed light on the interaction of the fibrillogenic polypeptide [1-93]ApoA-I with cellular membranes. It has to be noticed that interaction of unaggregated [1-93]ApoA-I with cell membranes represents a key event in the development of ApoA-I associated amyloidoses, but molecular details and consequences of this interaction are still largely unknown. We investigated the role of membrane fluidity by taking advantage of the use of Giant Unilamellar Vesicles (GUVs) as synthetic biomimetic systems. GUVs are spherical phospholipid bilayers entrapping a closed water-filled compartment [19], typically used to gain insight into membrane organization and response to external agents. Plasma membrane of eukaryotic cells may be considered as composed of small fluid domains, in which lipids are arranged in a liquid–crystalline phase nucleated within a continuous, more ordered gel phase [20]. Hence, in order to properly simulate these membrane phases, we used GUVs composed of two kinds of zwitterionic lipids endowed with different fluidity properties, such as dioleoylphosphatidylcholine (DOPC) and dipalmitoylphosphatidylcholine (DPPC). Since DOPC and DPPC melting temperatures are −16.5 °C and 41.3 °C, respectively, they are representative of the fluid-like state L_α (DOPC) and of the gel state L_β (DPPC) at room temperature (T = 24 °C) [21]. Analyses were performed by taking advantage of *Raman Tweezers* (RT) methodology, *i.e.* the combination of a Raman spectrometer and an Optical Tweezers (OT) [22]system [23]. This approach presents specific benefits with respect to well-consolidated techniques used to investigate membrane properties, such as Differential Scanning Calorimetry (DSC) [24], and fluorescence-based techniques [25,26]. As a matter of fact, RT can be used to trap and interrogate single objects, in order to provide information on their chemical components, without the need of sample labeling. Moreover, the analysis of Raman spectra is able to reveal molecular details of protein species/lipid interaction features. In particular, on the bases of selected Raman band changes, it is possible to identify the specific lipid moieties involved into the interaction with proteins. Furthermore, the use of OT allows the investigation of GUVs in the absence of any surface-induced spurious effect. Furthermore, RT allows the acquisition of the signal from a single GUV, thus giving the possibility to explore the heterogeneity of the system under investigation. In the present study, GUV manipulation by OT, combined with the non-destructive nature of Raman spectroscopy, gave us the opportunity to follow over time the interaction of single GUVs with the proteins under test. Being Raman spectra sensitive to molecular conformations, we were able to observe the reorganization of GUV phospholipid bilayer upon interaction with ApoA-I or with [1-93]ApoA-I. Interestingly, our results, besides revealing that [1-93]ApoA-I plays a key role in ruling ApoA-I interaction with membranes, indicate that the interaction of the fibrillogenic polypeptide with DPPC–GUVs has effects that resemble lipid phase transition induced by melting. Instead, the interaction with DOPC-based bilayers induces an alignment of membrane lipid chains, similar to that induced by cholesterol [27]. The same phenomena, even if significantly less pronounced, were observed for full-length ApoA-I.

2. Material and methods

2.1. Proteins under test

ApoA-I was purchased from Sigma-Aldrich (St Louis, MO, USA). [1-93]ApoA-I polypeptide was expressed and purified as previously described [16], omitting the neutralization step with ammonium hydroxide. The final yield of the procedure was estimated to be 2.5 mg/L of bacterial culture. Pure [1-93]ApoA-I was lyophilized and stored at −70 °C until use. For experimental purposes, the polypeptide was dissolved in the appropriate buffer and centrifuged before use.

2.2. Experimental set-up

The Raman analysis presented in this work was performed by using a combined Optical Tweezers and micro-Raman system. The set-up has been described in detail elsewhere [23,28]. Briefly, it consisted essentially in a home-made inverted microscope, endowed with a trapping beam (Nd:YAG, 1064 nm, Ventus 1064) and a Raman probe at 532 nm (Spectra Physics Millennia Xs). The microscope was equipped with a 100× objective lens (Olympus oil-immersion infinity corrected objective, 1.4 N.A.), in which both lasers were injected through a dichroic mirror, reflecting near-IR radiation and being transparent to visible radiation. The back-scattered photons followed back along the same optical pathway, reaching finally a holographic notch filter where the elastically scattered photons were suppressed. The resulting radiation was focused through a 50 μm aperture pinhole for confocal detection geometry and subsequently sent to a spectrometer (TRIAX 180, Jobin-Yvon) for the spectral analysis. The Raman radiation was detected by using a thermoelectrically cooled charge-coupled device (Pixis 100, Princeton Instruments), at the spectrometer exit. Raman spectra were acquired in the 900–1800 cm^{-1} spectral range. It should be noticed that the CH_2/CH_3 stretching bands in the 2800–3000 cm^{-1} region also provide information about the order of lipid architecture. However, in our case, the analysis of Raman bands in this region is complicated by the presence of the broad Raman bands in the 3000 cm^{-1} region due to H_2O. In fact, even if H_2O is a weak scatterer, Raman spectra of GUVs in aqueous solution present a significant contribution from water, due to the reduced scattering volume from the very thin (~5 nm) GUV membrane. The sample under investigation was placed in a chamber consisting of two 150 μm glass coverslips (Knittel Glasser, thickness no.1), sealed with parafilm stripes, which also act as an ~100 μm spacer. In order to maximize the GUV signal, the membrane was placed in the Raman confocal scattering volume by acting on the galvo-mirrors controlling the trapping laser beam position.

2.3. Data analysis

Principal Component Analysis (PCA) is a statistical tool that allows the decomposition of a multidimensional data set, in order to reduce its dimensionality while retaining the relevant characteristics contributing to most of its variance [29]. From a mathematical point of view, PCA is an orthogonal linear transformation that converts the original data (variables) into a new basis of uncorrelated coordinates (Principal Components, PCs), which are a linear combination of the original variables. PCs are ordered on the basis of their contribution to variation, with the first PC exhibiting the greatest contribution. The results of a PCA are given in terms of component scores and loadings. Loadings are the coefficients of the linear combination defining the PCs, in that they express the contribution of each original variable to the global variance of data set. Scores, instead, are the coordinates of the original data in the PC space. When PCA is applied to Raman spectra, the loadings enable the identification of the more relevant variables (*i.e.* wavenumbers), providing information on how they are correlated. Each score represents a whole spectrum plotted in a three dimensional space (score space), with points corresponding to similar spectra clustered together [30].

2.4. Preparation of DPPC– and DOPC–GUVs

GUVs were prepared following a procedure similar to that previously described [19]. Briefly, 3 mg of lipids (DOPC or DPPC) by Avanti were dissolved in 500 μL of chloroform (0.1 M). An aliquot (20 μL) of this solution was added to 200 μL of methanol and 980 μL of chloroform in a 50 mL round-bottom flask. Water (2.8 mL) was then slowly added alongside the flask walls. Finally, this solution was rotoevaporated for 3 min at a pressure of 10 mbar and a temperature of ~40 °C. This procedure provides vesicles whose diameter is in the range between 1 and 30 μm, as observed by bright field microscopy [31]. Vesicles with a diameter in the 4–8 μm range were selected for the experiments.

3. Results and discussion

As first, we acquired the Raman spectra of [1-93]ApoA-I and full-length ApoA-I in aqueous buffer. Fig. 1 shows the spectrum of a 0.76 μM [1-93]ApoA-I (*a*) and a 7.6 μM ApoA-I (*b*) aqueous solution in the spectral range between 900 and 1800 cm^{-1}.

Spectra were acquired by using a Raman probe power of 3 mW and an integration time $\tau = 30$ s. Under these experimental conditions, both signals exhibit only broad features due to the weak Raman bending mode around 1640 cm^{-1}, while no significant contribution from proteinaceous bands was detected, as a consequence of the low protein concentration. Trace *c* and *d* in Fig. 1 show, instead, the Raman spectra of an optically trapped DPPC– or DOPC–GUV, respectively, acquired under the same experimental conditions of traces *a* and *b* (no proteins added). The obtained Raman spectra present spectral features mainly arising from vibrations of the hydrocarbon chains, with minor contribution of polar groups. The assignment of the prominent peaks, reported in Table 1, has been performed on the basis of the criteria reported in [32–36].

According to these papers, the low-wavelength region is dominated by skeletal optical modes (SOM). These modes, being mainly C—C stretching vibrations delocalized along the entire acyl chain, provide information on the *intrachain* conformation. In particular, the relative intensity of trans/gauche peaks can be used to monitor the transition of a lipid to an ordered/disordered phase [37]. On the other hand, CH modes are essentially not coupled to the chain and are sensitive to lateral interactions inside the bilayer, so that the strength of these vibrations provides information on the *interchain* order. In particular, according to ref. [32], the decrease of the CH bending mode in CH_2 with respect to that in CH_3 is indicative of a reduced interchain order. In the case of DOPC–GUV spectrum, a strong feature at 1655 cm^{-1} takes into account the presence of the C═C bond. Obviously, the ratio of trans-to-gauche band intensity is larger for DPPC– than for DOPC–GUV, indicating that there is a higher degree of conformational order in the fully saturated lipid. After this preliminary step, we proceeded to investigate the interaction of [1-93]ApoA-I and ApoA-I with DPPC– and DOPC–GUVs. To this purpose, polypeptide and full-length protein were incubated with preformed GUVs at a protein:lipid molar ratio of ~1:100, up to 2 h (τ_{fin}). It should be noticed that, even at a lipid-to-protein molar ratio of 100:1, the lipid architecture can be significantly perturbed by proteins. As a matter of fact, due to the different sizes of proteins and lipids, protein–lipid interaction is not a one-to-one interaction. In particular, assuming for ApoA-I an effective diameter of 4.5 nm (estimated from its molecular weight, 28 kDa) and taking into account that head group area of one lipid molecule is ~0.71 nm^2, it is possible to estimate that ~25 lipid molecules directly interact with a single full-length protein. Moreover, it should be also noticed that both full-length protein and polypeptide can oligomerize in aqueous solution. In particular, ApoA-I exhibits an apparent hydrodynamic diameter of 11 nm in aqueous solution, which is consistent with the size of a protein dimer [38] This means that each dimer potentially interacts with ~130 lipid molecules. For this study, we acquired the Raman spectrum of 40 single, optically trapped GUVs at the initial state (τ_0) and at the end of incubation (τ_{fin}). Moreover, to follow the kinetics of lipid/protein

Table 1
Assignment of the prominent Raman features observed in DPPC– and DOPC–GUVs [32–34,36].

Wavenumber (cm^{-1})	Assignment
1063	SOM (trans)
1080	SOM (gauche)
1098	SOM (trans)
1128	SOM (trans)
1240	PO_2^- antisym stretch
1264	═C—H bend
1296	CH_2 twist
1440	CH bend in CH_2
1460	CH bend in CH_3
1655	C═C stretch
1735	C═O stretch

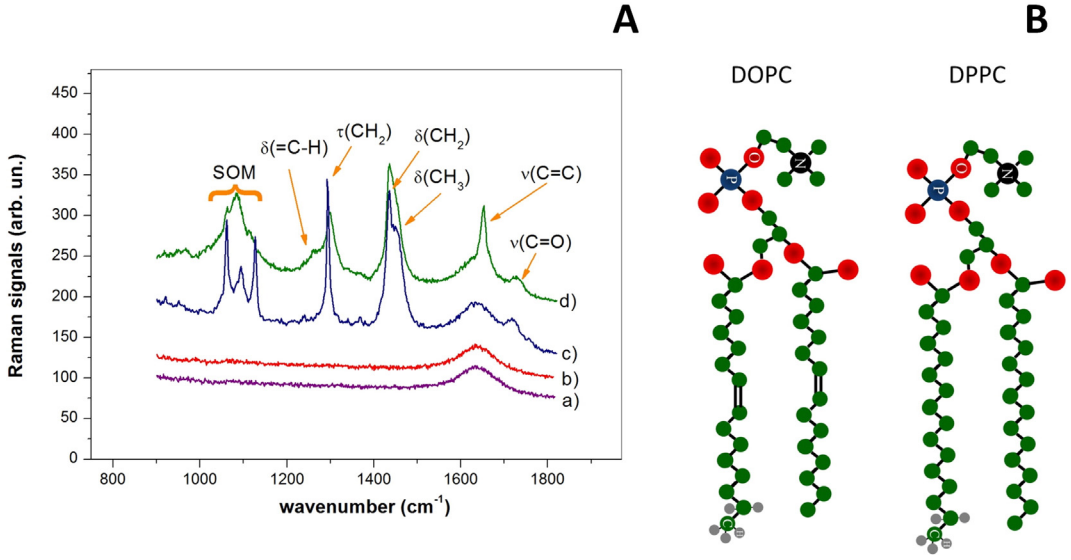

Fig. 1. Representative Raman spectra of proteins and lipids (DPPC and DOPC) under investigation. (A) Raman spectra of a 0.76 μM [1–93]ApoA-I (a) and a 7.6 μM full-length ApoA-I (b) aqueous solution in the spectral range between 900 and 1800 cm^{-1}. Spectra were obtained with an integration time of 30 s and a power of ~3 mW on the sample. c, d: single DPPC– (c) and DOPC–GUV (d) Raman spectra, acquired under the same experimental conditions in the absence of proteins. (B) Sketch of the chemical structure of DOPC and DPPC.

interaction, for 5 GUVs we performed a spectral interrogation every 2 min for the first 30 min, and then every 10 min up to 2 h. As a *control*, these analyses were performed on simple GUVs (no proteins added).

3.1. Interaction of [1-93]ApoA-I with DPPC–GUVs (gel phase)

Fig. 2A reports typical spectra of DPPC–GUVs analyzed upon incubation with the polypeptide (trace *a*) or the full-length protein (trace *b*), acquired at τ_{fin}.

Remarkably, quite relevant changes with respect to τ_0 were observed in both cases, even if more pronounced in the case of [1-93]ApoA-I. The main spectral changes involve the region 1170–1270 cm $^{-1}$, associated with interactions of the PO_2^- groups of the phospholipid polar head moiety, as well as regions 950–1100 cm $^{-1}$ and 1400–1480 cm $^{-1}$, which are sensitive to variations in the acyl chain order. The most striking differences specifically associated with the interaction of [1-93]ApoA-I with DPPC–GUVs lie in region 1170–1270 cm $^{-1}$. Actually, two additional bands are present around 1218 and 1240 cm $^{-1}$ and appear to be notably pronounced in the case of Raman spectra of DPPC–GUVs recorded in the presence of the fibrillogenic polypeptide. These bands are much less pronounced in the presence of ApoA-I and appear to be hardly visible in the absence of proteins (Fig. 1)[35]. According to literature [36], the aforementioned bands are associated with the asymmetric stretching vibrations of the PO_2^- groups. In particular, it has been previously reported that the antisymmetric stretching band lies around 1240 cm $^{-1}$ in dry DPPC–GUV and shifts to ~1220 cm $^{-1}$ in fully hydrated DPPC [36]. From Fig. 2, it is possible to note that lipid–protein interaction is responsible for a strong decrease of the *all-trans* band at 1128 cm $^{-1}$, as well as of the band at 1063 cm $^{-1}$ [37]. On the contrary, the *gauche* marker around 1080 cm $^{-1}$, generally associated with the presence of gauche chain segments [37], is significantly more pronounced upon DPPC–GUV interaction with the fibrillogenic polypeptide. This kind of spectral changes has been observed at a temperature almost corresponding to the lipid phase transition [32]. Under these conditions, lipid physical state passes from the ordered gel phase I_β (below T_c), where the hydrocarbon chains are fully extended and closely packed, to the more disordered I_α phase (above T_c), where the hydrocarbon chains are randomly oriented and fluid. In agreement with this, the band around 1440 cm $^{-1}$ appears to be weakened with respect to that around 1460 cm $^{-1}$, which is indicative of a reduced lateral packing, and a consequent more disordered lipid chain architecture [32,34]. To better assess the differences between the three analyzed samples, we evaluated the intensity of the most prominent peaks involved in spectral changes by performing a fitting with a multi peak Gaussian function in all the aforementioned regions. In particular, to properly take into account the presence of all spectral features, we used a 4 Gaussian convolution for 950–1100 cm $^{-1}$ region, a 2 Gaussian convolution for 1170–1270 cm $^{-1}$ region and a 2 Gaussian convolution for 1400–1480 cm $^{-1}$ region. In all the cases, a fourth order polynomial curve was added in order to take into account a residual background not completely removed by the subtraction of the background signal. In Fig. 2B, we show a typical result of the fitting procedure for one of the spectra acquired for the polypeptide in the 950–1100 cm $^{-1}$ region, at $\tau = 0$ and $\tau = \tau_{fin}$. The same procedure was used for all the GUV spectra acquired for the three investigated samples. Some significant outcomes of this procedure are reported in Fig. 2C.

In more detail, panel *i*) reports the mean values of $\alpha = (I_{1218} + I_{1240})$, *i.e.* the integrated area under the two aforementioned PO_2^- stretching bands, along with the standard deviations over the 40 GUV spectra. As mentioned above, this parameter fully differentiates the analyzed samples, highlighting the ability of the polypeptide to interact with the

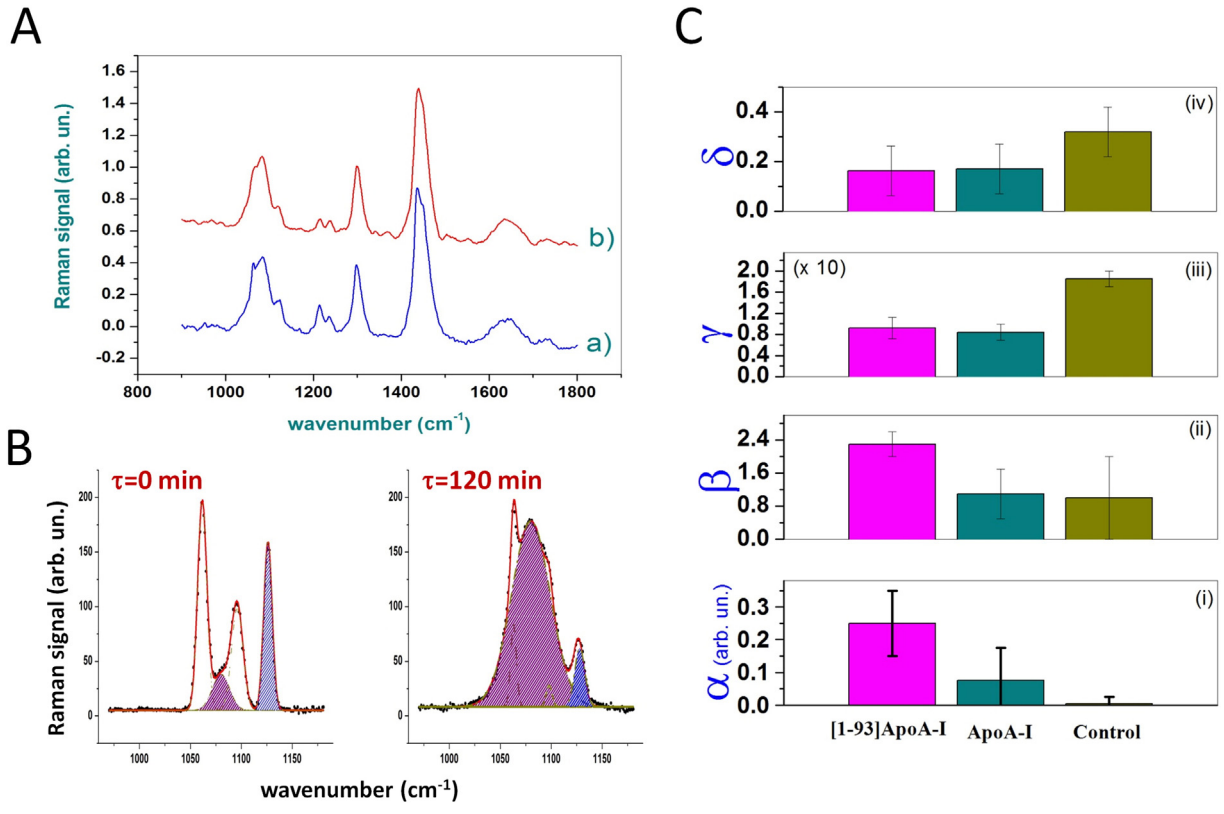

Fig. 2. Analysis of the interaction of ApoA-I and [1-93]ApoA-I with DPPC GUVs. (A) Typical normalized Raman signals of DPPC GUVs upon incubation with [1-93]ApoA-I (trace *a*) or full-length protein (trace *b*), acquired at τ_{fin} (120 min). (B) Representative fitting curves for a spectrum of the polypeptide in the region 950–1100 cm^{-1}. The dotted lines represent the separate contributions of the four Gaussian curves used as fit functions. Moreover, hatched areas correspond to the integrated area under the peaks used for evaluation of γ. (C) α (*i*), β (*ii*), γ (*iii*) and δ (*iv*) mean values obtained by the fitting procedure are exemplified in panel B. The error bars correspond to the standard deviations over the 40 spectra analyzed for each sample.

polar heads of DPPC. A similar behavior, although at a much lesser extent, was recorded for the full-length protein. As a matter of fact, it is reasonable to think that the polypeptide interacts with the PO $\bar{2}$ bond in a manner that induces some modifications of the PO $\bar{2}$ bond polarizability, responsible for the enhanced Raman activity. It should be also pointed out that, differently from the polypeptide sample, the spectra corresponding to the ApoA-I–GUV complex present a consistent fluctuation of the ratio $\beta = I_{1218}/I_{1240}$, as reported in Fig. 2C, panel *ii*. This is clearly suggestive of a random protein positioning in the lipid head region, which gives rise to a different environment for the PO $\bar{2}$ bond. Intriguingly, in this frame, the lower β value for ApoA-I with respect to [193]ApoA-I could be ascribed to a lower exposure to solvent of the PO $\bar{2}$ bond in the case of full-length protein with respect to its fragment. The two additional parameters reported in Fig. 2C, namely the ratios $\gamma = I_{1128}/I_{1080}$ (panel *iii*) and $\delta = I_{1440}/I_{1460}$ (panel *iv*), are indicative of the protein/polypeptide interaction with the lipid acyl chains. As discussed above, their decrease with respect to the pure lipid case is indicative of a reduced order for the acyl chain assembly. In particular, the similar γ and δ values obtained in our analysis clearly prove that the polypeptide shares with the full-length ApoA-I protein the ability to interact with the lipid membrane bilayer. This, in turn, is likely due to the presence, in both protein and fragment helices, of a non-polar side, clearly prone to be buried into the hydrophobic region of the bilayer. Notably, our observations are in agreement with recently published data indicating that 1-83 ApoA-I peptide, which is part of [1-93]ApoA-I analyzed herein, contains four most probable membrane-binding regions [39]. Globally, these observations let us hypothesize that the ApoA-I N-terminal fibrillogenic domain is responsible for protein/fibril attachment to the surface of lipid vesicles.

Interestingly, all the spectral modifications induced by both polypeptide and full-length protein are detected very early (within ~5 min), reaching a steady state within 20 min. Fig. 3A reports the time evolution of γ obtained for a single optically trapped DPPC–GUV interacting with [1-93]ApoA-I. A similar evolution has been observed also for the other parameters evaluated herein, as well as for GUVs upon interaction with ApoA-I. In both cases, their behavior resembles a sigmoidal curve, with a transition in the 10–30 min region. This indicates that the interaction of both the fibrillogenic polypeptide and the full-length protein with DPPC–GUVs have effects that resemble the lipid phase transition induced by melting, which are much more pronounced in the case of the fibrillogenic polypeptide [32]. This observation could be also verified by using DSC on a statistically significant number of GUVs. However, it has to be noticed that, in the case of the approach herein proposed, sample heterogeneity is completely masked.

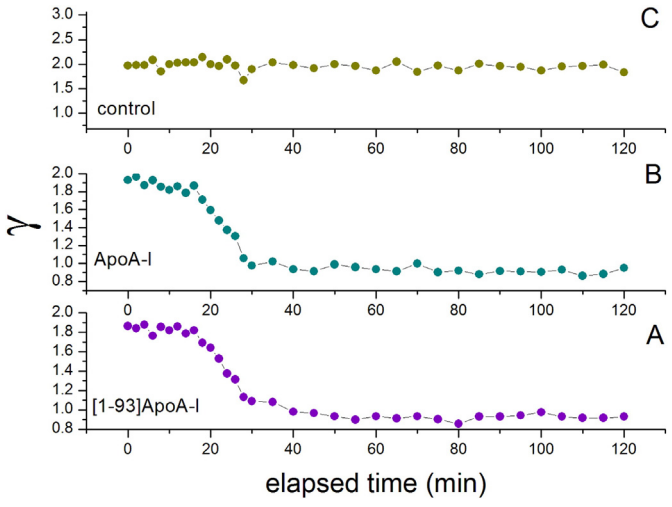

Fig. 3. Kinetic analysis of protein–DPPC GUV interaction. Time evolution of observed gamma for a single, optically trapped DPPC–GUV interacting with the polypeptide (A), the full-length protein (B) and in the absence of proteins (C).

3.2. Interaction of [1-93]ApoA-I with DOPC–GUVs (liquid phase)

As mentioned above, the effect of ApoA-I fibrillogenic fragment on the fluid membrane phase was explored by analyzing its interaction with DOPC–GUVs at room temperature (~24 °C). However, different from the DPPC–GUVs case, the spectroscopic effect of this interaction was not immediately detectable. Although, in principle, this could be ascribed to a weak lipid–protein interaction, we argued that this could be likely due to the obvious difficulty in identifying protein effects in a relatively disordered structure. Therefore, in order to appreciate the fine tuning of DOPC–GUV spectra upon interaction with proteins, we choose to analyze our set of data by Principal Component Analysis (PCA). PCA was performed by using a home-made *MATLAB*, *MathWorks* software, based on the use of the *princomp* routine. Before analysis, Raman spectra were pre-processed by removing a fourth-order polynomial curve and eliminating spurious signals deriving from cosmic ray contributions. Spectra were also normalized and mean centered before the decomposition in PCs.

Fig. 4 shows the three-dimensional score plot obtained by analyzing the 120 spectra for the first 3 PCs, which globally take into account almost 92% of the total spectra variability (see Fig. 4B) In the score plot, the symbols corresponding to [1-93]ApoA-I–GUV and ApoA-I–GUV complexes are triangles and squares, respectively, while spectra corresponding to GUVs are represented by dots. Interestingly, points corresponding to the spectra of each sample tend to be clustered together, with some overlapping between the two protein-containing systems. Most of data variability (~75%) is taken into account by PC1. Notably, PC1 scores of the samples containing the polypeptides and the full-length protein are quite apart from the pure GUV sample, which, instead, occupy a score plot region of relatively low PC1 score values. The reason of this differentiation can be figured out by PC1 loading inspection (Fig. 5A) This loading exhibits main features at around 1655 cm^{-1}, associated with olefinic vibrations of unsaturated chain segments.

In particular, they appear as negative peaks, with some overlapping with dispersive-like features, indicative of a shift to lower wavenumbers of the corresponding Raman peaks. According to literature [40], a shift of olefinic vibration to lower wavenumbers can be indicative of an elongation of the C═C bond. Therefore, positive PC1 scores correspond to spectra of lipid structures where C═C bond is weakened (negative load features) and/or elongated (dispersive load features). As PC1, also PC2 component provides differentiation between the two protein-containing systems and the pure DOPC–GUVs, although points corresponding to the first two samples occupy the same score plot region. As a matter of fact, the main features of PC2 loading lie in the region around 1450 cm^{-1}, including the two CH modes around 1440 cm^{-1} and 1460 cm^{-1}. Clearly, the simultaneous presence of a positive feature around 1440 cm^{-1} and a negative feature around 1460 cm^{-1} suggests that higher PC2 score values correspond to more ordered lipid structures. Interestingly, the improved acyl chain order seems to be somewhat related to the shift of olefinic band highlighted by PC1 loading. In particular, a more ordered acyl chains configuration could result from a higher interchain pressure, giving rise to a repulsion between chains lying at opposite sides of the C═C bonds and, as a consequence, to a C═C bonding elongation. The last PC herein analyzed, PC3, takes into account about 10% of the total data variability. As for PC2, this component highlights differences between spectra of pure DOPC with respect to the two protein-containing systems, with the latter exhibiting PC3 scores spread out through PC3 score axis. However, the mean PC3 score is higher for [1-93]ApoA-I (triangles) than for full-length ApoA-I (squares), therefore suggesting a more pronounced effect of [1-93] ApoA-I with respect to the full-length protein on the lipid membrane (Fig. 4A). PC3 loading is quite complex, presenting both positive and

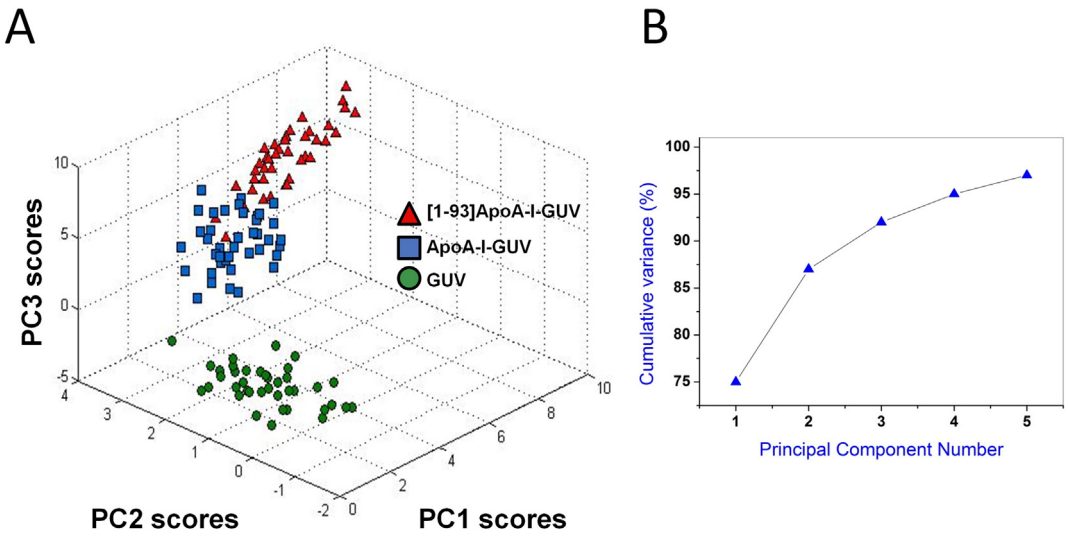

Fig. 4. PC analysis of DOPC–GUVs upon interaction with ApoA-I fibrillogenic polypeptide or the full-length protein. (A) Score plot relative to the PC analysis of DOPC–GUV spectra acquired at τ_0. Points corresponding to [1-93]ApoA-I–GUV complexes and ApoA-I–GUV spectra are represented by triangles and squares, respectively, while spectra corresponding to GUVs in the absence of proteins are represented by dots. (B) Cumulative variance for the first 5 PCs.

negative features. The prominent positive peak is around 1440 cm $^{-1}$, in close proximity with a negative feature at 1460 cm $^{-1}$, and this, as for PC2, can be read in terms of a higher interchain order. Notably, PC3 loading also exhibits relatively sharp bands at 1063 and 1128 cm $^{-1}$, which are all correlated to C—C vibrations of *trans* isomers, indicating that the increase in PC3 scores implies an increased number of trans isomers. The corresponding decrease of gauche isomers is, instead, pointed out by the negative load peak at ~1080 cm $^{-1}$. Therefore, PC3 highlights the presence of lipid structures characterized by a higher order in both intermolecular and intramolecular acyl chains.

As for the DPPC case, we also analyzed the time evolution of single, optically trapped GUVs. However, in this case, the time evolution was followed by PC analysis of single GUVs spectrally interrogated while interacting with polypeptides/proteins (no meaningful data can be extracted for DOPC-–GUVs in aqueous buffer) Fig. 6 reports the PC1 score evolution for the two protein-containing samples. Interestingly, both sets of data suggest a faster interaction with respect to DPPC–GUVs, with a *steady state* reached upon 10 min incubation. This outcome could be due to the higher fluidity of DOPC bilayer.

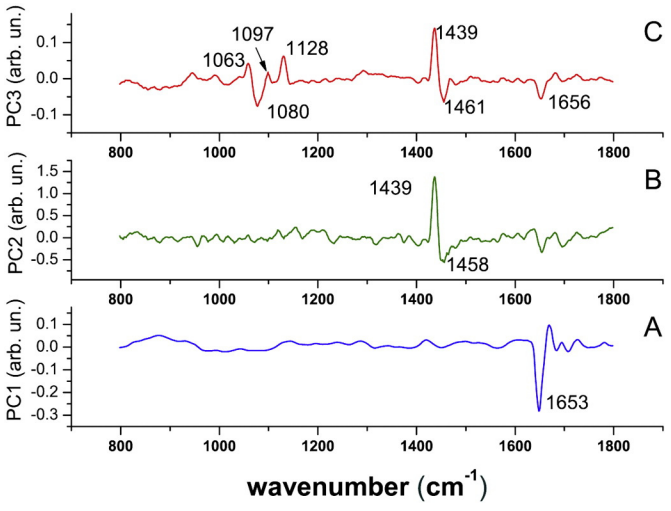

Fig. 5. Analysis of the interaction of ApoA-I and [1-93]ApoA-I with DOPC–GUVs by PCA. PC1-, PC2- and PC3-loading plot (curves A, B and C, respectively) resulting from the analysis of all the 120 GUV spectra.

4. Conclusions

Globally, our results indicate that the interaction features of [1-93]ApoA-I with eukaryotic membranes strongly depend on the lipid phase. In particular, ApoA-I N-terminal fibrillogenic polypeptide was found to induce a conformational disorder in ordered gel lipid bilayers. In addition, the fibrillogenic polypeptide was also found to induce changes in vibrations close to the polar part of phospholipids, in particular in PO_2^- stretching band. On the basis of this observation, we conjecture that a significant portion of [1-93]ApoA-I molecules is not deeply buried inside the bilayer, but remains in close proximity to the membrane–water interface. Similar effects, even if significantly less pronounced, were observed when DPPC–GUVs were incubated with full-length ApoA-I.

We also provide evidence that [1-93]ApoA-I is able to interact with liquid-like lipid bilayers, simulated by DOPC–GUVs. In this case, we analyzed our data set by PCA and demonstrated that [193]ApoA-I polypeptide can reside within the lipid bilayer, inducing an additional pressure between adjacent lipid chains. This limits chain movements and favors the more *ordered* CH bending mode in CH_2 with respect to that in CH_3. We also observed a reduction of C═C band, probably ascribed to

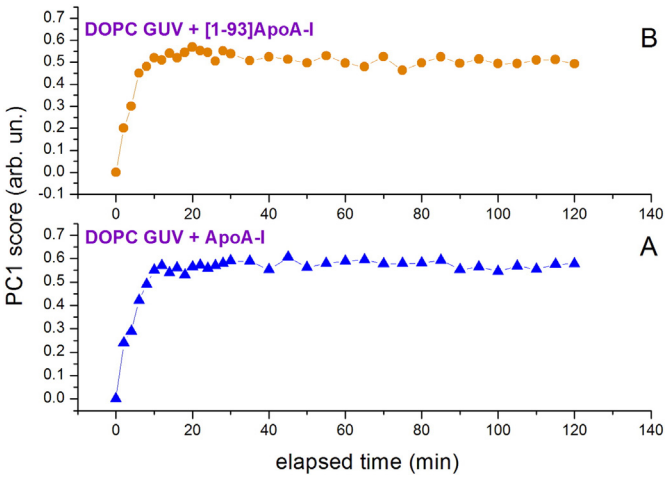

Fig. 6. Kinetic analysis of protein–DOPC–GUV interaction. PC1-score time evolution for a single optically trapped GUV interacting with [1-93]ApoA-I (A) and ApoA-I (B) molecules.

reduced mobility of C═C bonds due to the peptide residence in the *kink* region of lipid chains. Interestingly, our analyses on DOPC-–GUVs suggest the absence of a significant interaction of either [1-93]ApoA-I or ApoA-I with lipid polar heads. This could indicate that, in the fluid (L_α) phase, protein species tend to penetrate the membrane bilayer, instead of remaining in proximity to the lipid–water interface. This observation is also in agreement with the reported existence of plasma membrane areas endowed with high affinity for full-length ApoA-I [41], as well as with our previous results indicating that [1-93]ApoA-I polypeptide is efficiently internalized and subsequently degraded in target cells [42]. To our knowledge, the ability of the polypeptide to penetrate membrane fluid phases inducing an alignment of lipid chains has not been previously described. This indicates that the polypeptide may alter the bilayer mechanical stability, with effects similar to those induced by cholesterol [43–45], an event that might play an important role in the development of the pathology.

Globally, our observations, revealing the specific ability of a natively unfolded pathogenic polypeptide to insert in, and possibly to cross cell membranes, provide a contribute to shed light on the intriguing and still largely unknown molecular level details of its interaction with biological membranes.

References

[1] J. Fantini, N. Yahi, Expert Rev. Mol. Med. 12 (2010) e27.
[2] G. Shanmugam, R. Jayakumar, Biopolymers 76 (2004) 421–434.
[3] A. Kakio, Y. Yano, D. Takai, Y. Kuroda, O. Matsumoto, Y. Kozutsumi, K. Matsuzaki, J. Pept. Sci. 10 (2004) 612–621.
[4] X. Hou, S.J. Richardson, M.I. Aguilar, D.H. Small, Biochemistry 44 (2005) 11618–11627.
[5] A. Abedini, D.P. Raleigh, Protein Eng. Des. Sel. 22 (2009) 453–459.
[6] M. Zhu, A.L. Fink, J. Biol. Chem. 278 (2003) 16873–16877.
[7] L. Obici, G. Franceschini, L. Calabresi, S. Giorgetti, M. Stoppini, G. Merlini, V. Bellotti, Amyloid 13 (2006) 191–205.
[8] L. Obici, V. Bellotti, P. Mangione, M. Stoppini, E. Arbustini, L. Verga, I. Zorzoli, E. Anesi, G. Zanotti, C. Campana, M. Vigan, G. Merlini, Am. J. Pathol. 155 (1999) 695–702.
[9] M. Eriksson, S. Schönland, S. Yumlu, U. Hegenbart, H. von Hutten, Z. Gioeva, P. Lohse, J. Buttner, H. Schmidt, Röcken C., J. Mol. Diagn. 11 (2009) 257–262.
[10] E. Adachi, A. Kosaka, K. Tsuji, C. Mizuguchi, H. Kawashima, A. Shigenaga, K. Nagao, K. Akaji, A. Otaka, H. Saito, FEBS Lett. 588 (2014) 389–394.
[11] X. Mei, D. Atkinson, J. Biol. Chem. 286 (2011) 38570–38582.
[12] D.W. Borhani, D.P. Rogers, J.A. Engler, C.G. Brouillette, Proc. Natl. Acad. Sci. U. S. A. 94 (1997) 12291–12296.
[13] P.S. Chetty, L. Mayne, S. Lund-Katz, D. Stranz, S.W. Englander, M.C. Phillips, Proc. Natl. Acad. Sci. U. S. A. 106 (2009) 19005–19010.
[14] P. Mangione, M. Sunde, S. Giorgetti, M. Stoppini, G. Esposito, L. Gianelli, L. Obici, Protein Sci. 10 (2001) 187–199.
[15] S. Di Gaetano, F. Guglielmi, A. Arciello, P. Mangione, M. Monti, D. Pagnozzi, S. Raimondi, S. Giorgetti, S. Orrú, C. Canale, P. Pucci, C.M. Dobson, V. Bellotti, R. Piccoli, Biochem. Biophys. Res. Commun. 351 (2006) 223–228.
[16] D.M. Monti, F. Guglielmi, M. Monti, F. Cozzolino, S. Torrassa, A. Relini, P. Pucci, A. Arciello, R. Piccoli, Eur. Biophys. J. 39 (2010) 1289–1299.
[17] P.G. Frank, Y.L. Marcel, J. Lipid Res. 41 (2000) 853–872.
[18] M. Tanaka, P. Dhanasekaran, D. Nguyen, S. Ohta, S. Lund-Katz, M.C. Phillips, H. Saito, Biochemistry 45 (2006) 10351–10358.
[19] A. Moscho, O. Orwar, D.T. Chiu, B.P. Modi, R.N. Zare, Proc. Natl. Acad. Sci. U. S. A. 93 (1996) 11443–11447.
[20] Y. Sun, M. Hao, C.P. Liang, D.L. Silver, C. Cheng, F.R. Maxfield, A.R. Tall, J. Biol. Chem. 278 (2003) 5813–5820.
[21] Z.V. Leonenko, E. Finot, H. Ma, T.E.S. Dahms, D.T. Cramb, Biophys. J. 86 (2004) 3783–3793.
[22] N. Malagnino, G. Pesce, A. Sasso, E. Arimondo, Opt. Commun. 214 (2002) 15–24.
[23] G. Rusciano, A.C. De Luca, G. Pesce, A. Sasso, Anal. Chem. 79 (2007) 3708–3715.
[24] R.N. McElhaney, Biochim. Biophys. 864 (1986) 361–421.
[25] W. Hohlweg, S. Kosol, K. Zangger, Curr. Protein Pept. Sci. 13 (2012) 267–279.
[26] T. Parasassi, E.K. Krasnowska, L. Bagatolli, E. Gratton, J. Fluoresc. 8 (1988) 365–373.
[27] T.M. Ferreira, F. Coreta-Gomes, O.H. Samuli Ollila, M.J. Moreno, W.L.C. Vaz, D. Topgaarda, Phys. Chem. Chem. Phys. 15 (2013) 1976–1989.
[28] G. Rusciano, A.C. De Luca, G. Pesce, A. Sasso, Carbon 47 (2009) 2950–2957.
[29] I.T. Jolliffe, Principal Component Analysis, Springer Verlag, Berlin, 2002.
[30] G. Rusciano, Phys. Med. 26 (2010) 233–239.
[31] A.G. Lee, Lipid-protein interactions in biological membranes: a structural perspective, Biochim. Biophys. Acta 1612 (2003) 1–40.
[32] B.P. Gaber, P. Yanger, W.L. Peticolas, Biophys. J. 21 (1978) 161–176.
[33] B.P. Gaber, W.L. Peticolas, Biochim. Biophys. Acta 465 (1977) 260–274.
[34] Z.D. Schultz, I.W. Levin, Annu. Rev. Anal. Chem. 4 (2011) 343–366.
[35] Parker, F.S. Applications of Infrared, Raman and Resonance Raman Spectroscopy in Biochemistry, Plenum Press, New York and London.
[36] J.L.R. Arrondo, F.M. Goñi, Chem. Phys. Lipids 96 (1998) 53–68.
[37] T. Gilman, Kauffman J.W., H.J. Pownall, Biochemistry 20 (1981) 656–661.
[38] R. Del Giudice, A. Arciello, F. Itri, A. Merlino, M. Monti, M. Buonanno, A. Penco, D. Canetti, G. Petruka, S.M. Monti, A. Relini, P. Pucci, R. Piccoli, D.M. Monti, Biochim. Biophys. Acta 1860 (2016) 434–444.
[39] V. Trusova, G. Gorbenko, M. Girych, E. Adachi, C. Mizuguchi, R. Sood, P. Kinnunen, H. Saito, J. Fluoresc. 25 (2015) 253–261.
[40] P.T.T. Wong, H.H. Mantsch, Biophys. J. 54 (1988) 781–790.
[41] S.A. Sánchez, M.A. Tricerri, G. Ossato, Gratton. E., Biochim. Biophys. Acta 1798 (2010) 1399–1408.
[42] A. Arciello, N. De Marco, R. Del Giudice, F. Guglielmi, P. Pucci, A. Relini, D.M. Monti, R. Piccoli, J. Cell. Mol. Med. 15 (2011) 2652–2663.
[43] D.A. Pink, T.J. Green, D. Chapman, Biochemistry 19 (1980) 349–356.
[44] P.F. Almeida, Biophys. J. 100 (2011) 420–429.
[45] M.J.L. de Lange, M. Bonn, M. Muller, Chem. Phys. Lipids 146 (2007) 76–84.